ACS APPLIED MATERIALS & INTERFACES

www.acsami.org

Research Article

Humidity-Responsive Shape Memory Polyurea with a High Energy Output Based on Reversible Cross-Linked Networks

Wen Liu, Yang He, and Jinsong Leng*

Cite This: *ACS Appl. Mater. Interfaces* 2023, 15, 2163−2171

Read Online

ACCESS | Metrics & More | Article Recommendations | Supporting Information

ABSTRACT: High-performance shape memory polymers with multifunctions are essential in sensors, wearable flexible electronics, artificial muscle actuators, and reversible morphing structures. In this work, a transparent and humidity-responsive shape memory polyurea featuring a high tensile strength (51 MPa), a high recovery stress (12 MPa) with an high energy output (0.98 J/g), and tolerance to extreme environments (retains great malleability at −196 °C) is prepared through constructing a bioinspired hard−soft nanophase structure and through hierarchical hydrogen bonding in the molecular network. The hard segment of a strong hydrogen bonding region is in charge of humidity-responsive behavior, and the soft segment of a weak bonding region provides the flexibility of the molecular chain. Furthermore, the periodicity of the phase-separated domains is 12 nm as characterized by small-angle X-ray scattering. The hydrogen bonding cross-linked network can be opened under the action of stress and re-bonded by heating, just like a zipper structure of reversible linking property. This unique molecular structure contributes to the humidity-responsive behavior of polyurea rolling up 160° in 20 s on the palm, as well as a high energy output lifting a 100 g weight exceeding 1631 times its own mass to 60 mm. The molecular structure of the hard−soft nanophase and the hierarchical hydrogen bonding offer an effective approach toward achieving a high-performance shape memory polymer with humidity-sensitive functions.

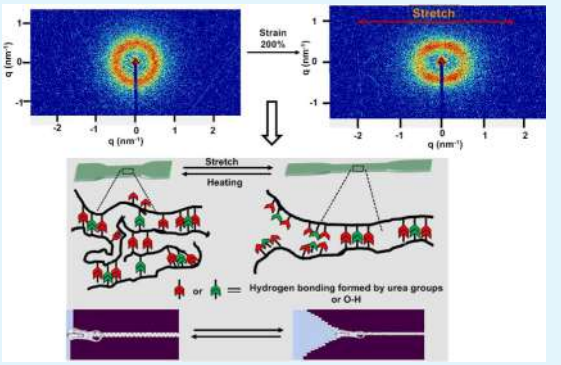

KEYWORDS: *high-performance shape memory polymers, polyurea, hydrogen bonding, humidity response, energy output*

1. INTRODUCTION

Thermo-triggered shape memory polymers (SMPs) are one of the most popular smart materials owing to their controllable shape transformation, large deformation, and hysteresis-free shape recovery. Furthermore, heat energy can be generated by an electric field, light, and a magnetic field to implement remote control of the shape-changing module; therefore, thermo-triggered SMPs are applied in space-inflatable structures,[1] left atrial appendage occluders,[2] organic electronic devices,[3,4] and artificial muscles.[5] However, most SMPs are not competitive in energy density (<1 MJ/m^3) and shape recovery stress (<5 MPa),[6] limiting their use in mechanical work applications.[7] The shape recovery stress is generated in returning from the temporary shape to the original shape, and its value is determined by the stored entropic energy that is produced in the programming temporary process.[8] The energy work output is determined by the shape recovery stress and recovery strain.[9] Therefore, the construction of molecular network structures of SMPs with a high energy output must balance the strength, toughness, and ability to reversibly recover after large strain.

Natural materials possess excellent mechanical properties and stimuli response owing to their intricate and hierarchical structure, such as hierarchically ordered hard and soft phases,[10−12] and miraculous noncovalent interactions.[13] In detail, the hierarchical structure including the β-sheet nanocrystals and the amorphous phase endow spider silk with remarkable high strength, toughness, and great elasticity. Besides, many plants will be able to change their shape according to environmental stimuli, such as mimosa. The systolic and diastolic function of mimosa is attributed to a periodic nanostructure.[14] Inspired by natural structural materials, many groundbreaking research studies have been reported, such as record-high mechanical robustness of poly(urethane-urea) elastomers,[15] artificial muscle fibers,[10] and reversible morphing hydrogels.[16] These high-performance and multifunctional shape-changing polymers are promising in soft actuators, artificial muscles, biological medical devices, and large self-unfolding structures in extreme environments.

Humidity-responsive polymers with reversible shape-changing behavior, high response sensitivity, fast shape-changing ability, and environmentally friendly driving energy[17,18] are

Received: October 13, 2022
Accepted: December 14, 2022
Published: December 26, 2022

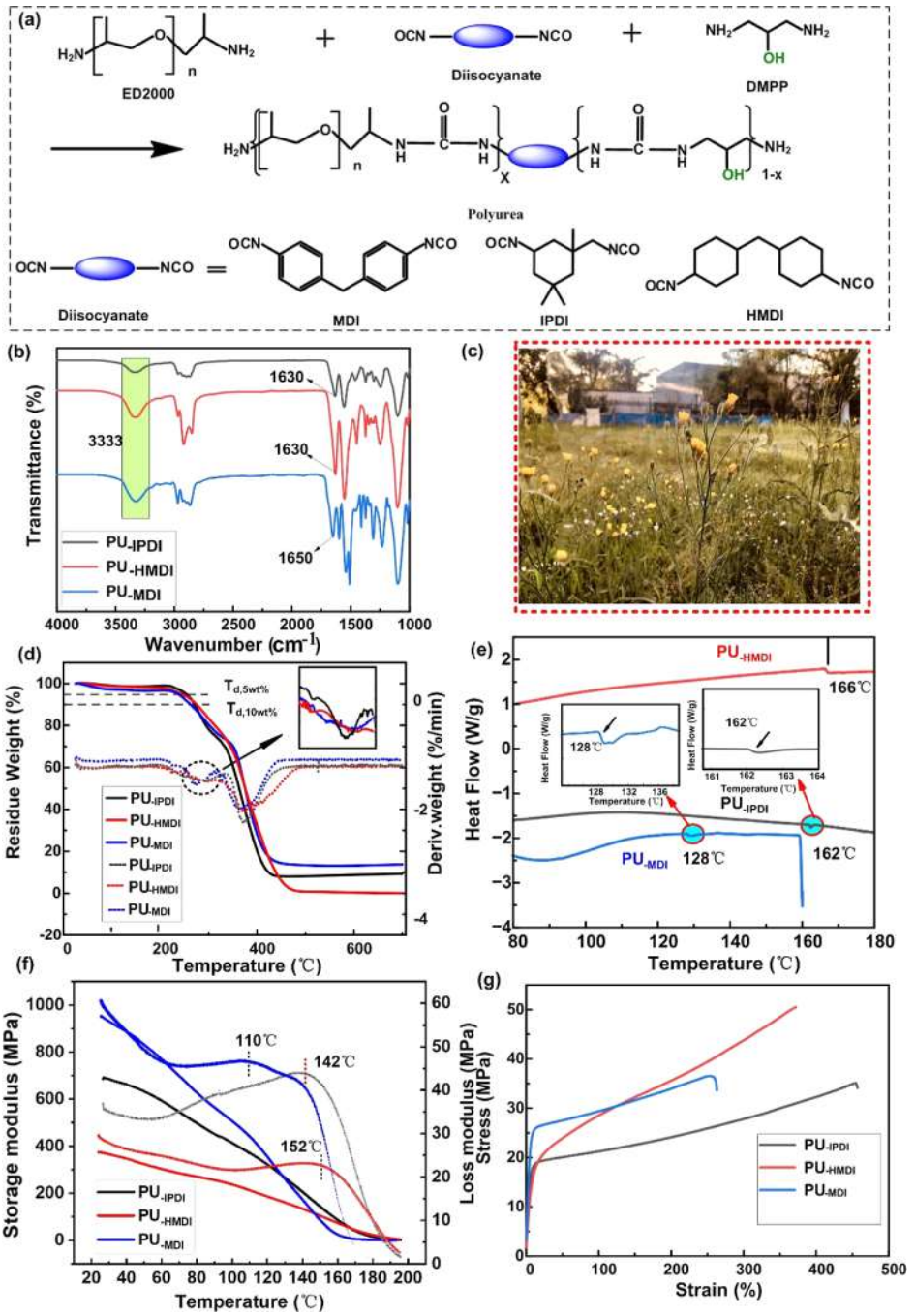

Figure 1. (a) Synthesis and chemical structures of PUs. (b) FT-IR curve of three PUs. (c) Photograph of a 0.3 mm-thick PU_{-HMDI} sheet. (d,e) TGA, DTG, and DSC thermograms of PUs under a N_2 atmosphere. (f) Storage and loss modulus curves of PUs. (g) Stress−strain curves of PUs.

promising in the fields of soft robots,[19] humidity sensors,[20] artificial muscles,[21] and anticounterfeit labels.[3] Nevertheless, previous humidity-responsive materials mainly including MXene,[22,23] graphene oxide,[24] and cholesteric cellulose[3,22,25] possess limited transparency and mechanical properties.[26] The development of SMPs with intrinsic humidity response remains much less explored.[27]

Considering that most of the shape-changing SMPs have a low energy output and are generally irreversible, while the humidity-responsive behavior is reversible, we engineer a unique molecular structure for the preparation of a humidity-responsive shape memory polyurea (PU), possessing high shape recovery stress, large energy work output, excellent mechanical robustness, and extreme low-temperature resistance. The molecular network of PU is constituted through introducing a bioinspired hard−soft nanophase structure and through hierarchical hydrogen bonding to achieve the excellent combination of multifunction and excellent mechanical property. The hard segments are constructed to provide a stronger hydrogen bonding network and humidity-responsive groups to endow the material with strength and multifunction. Concurrently, we directly introduce O−H into the side chain to obtain intrinsic humidity response, high transparency, and great mechanical properties. Polyetheramine 2000 (ED2000) with excellent flexibility is employed as a soft segment to provide flexibility and low-temperature resistance. The hierarchical hydrogen bonding

https://doi.org/10.1021/acsami.2c18489
ACS Appl. Mater. Interfaces 2023, 15, 2163−2171

Table 1. Mechanical Properties of the PU Plastic

polyureas	$T_{d,5wt\ \%}$(°C)	$T_{d,10wt\ \%}$(°C)	storage modulus (MPa)	tensile strength (MPa)	strain (%)	$T_g{}^a$ (°C)	$T_g{}^b$ (°C)
PU_{-IPDI}	252	272	685	35	454	162	142
PU_{-HMDI}	244	276	366	51	372	166	152
PU_{-MDI}	235	260	951	36	255	128	110

^aT_g is acquired by DSC. ^bT_g is acquired by DMA.

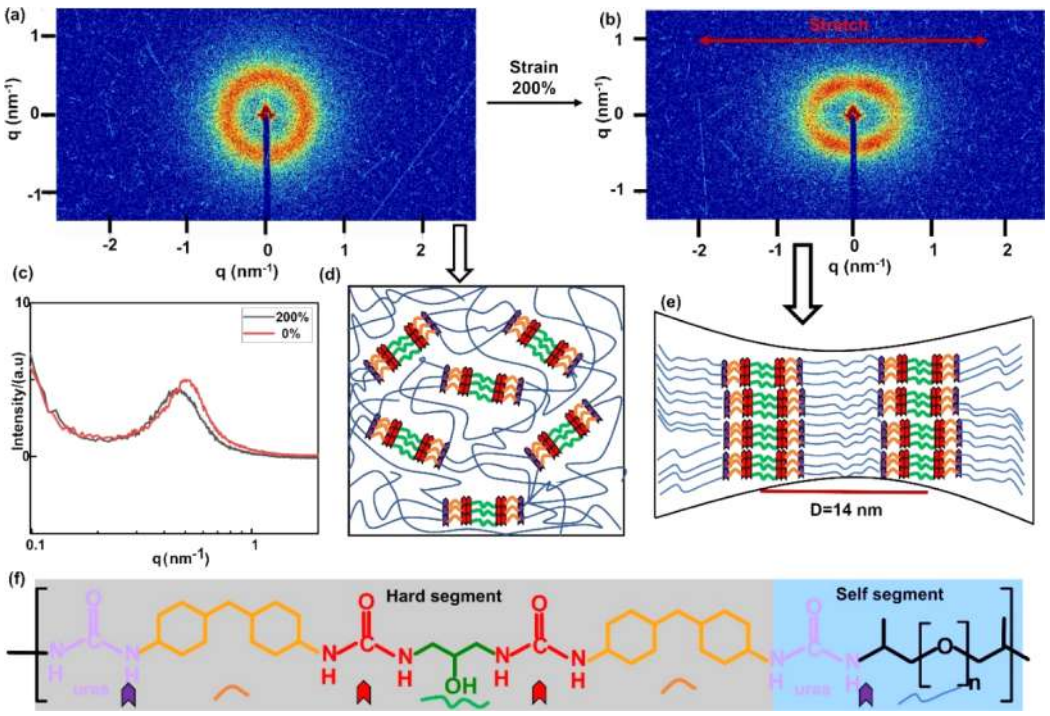

Figure 2. 2D SAXS of PU_{-HMDI} at 0% (a) and 200% (b) strains. (c) 1D SAXS intensity profiles of PU_{-HMDI} at 0 and 200% strains. (d) Schematic diagram of a random coil model of PU_{-HMDI} at 0% strain. (e) Schematic diagram of orientation of PU_{-HMDI} at 200% strain along the stretching direction. (f) Molecular structural formula of PU_{-HMDI}.

cross-linked networks enhance steric hindrance and interaction within polyurea, contributing to high shape recovery stress and energy output. Moreover, the networks are able to open under strain and also recombine by heating, indicating that the hierarchical hydrogen bonding (H-bonding) networks can be the same as that of a zipper.

2. RESULTS AND DISCUSSION

2.1. Structural and Mechanical Property Analysis. As shown in Figure 1a, the synthetic routes of PU_{-IPDI}, PU_{-HMDI}, and PU_{-MDI} could be clearly acquired. ED2000, possessing high flexibility, is selected as a flexible chain to improve toughness, and indispensably, DMPP is selected as a chain extender to ensure the rigidity of PUs and contributes to the humidity-responsive group (O−H). In Figure 1b, to confirm the formation of PUs, the FT-IR curves of three PUs are presented. The characteristic peak positions of the three PUs are basically the same, which indicates that they have the same groups. In detail, 3333 and 1630−1689 cm^{-1} are ascribed to the N−H and C═O groups of the urea group, proving the formation of PUs.[28] Further, the peak of O−H is possible to overlap with the peak of N−H at 3333 cm^{-1}. Particularly, the peaks of C═O groups of PU_{-IPDI} and PU_{-HMDI} appearing at 1630 cm^{-1} and that of PU_{-MDI} appearing at 1650 cm^{-1} are different because the degree of H-bonding association leads to different stretching vibrations, impacting the peak position of C═O. The peak of C═O groups appears at 1630 cm^{-1}, confirming the formation of ordered H-bonding. Obviously, the peak of C═O groups appears at 1650 cm^{-1}, indicating the unordered H-bonding only existing in PU_{-MDI}. Particularly, the peak of free C═O groups is ascribed to 1670−1689 cm^{-1},[29] but there is no peak in this range, indicating that the C═O groups in the PU system are almost associated to form H-bonding. The peak intensity of the H-bonded N−H and C═O groups of PU_{-HMDI} compared with that of PU_{-IPDI} and PU_{-MDI} is the strongest, which is shown in Figures S1 and S2, respectively. Further, PU_{-IPDI}, PU_{-HMDI}, and PU_{-MDI} possess great transparency like glass. For example, the transparency of PU_{-HMDI} is shown in Figure 1c, and we can clearly see the garden scenery through the PU_{-HMDI} film, as transparent as glass. Thermogravimetric analysis (TGA) is employed to test the thermal stability of PUs as shown in Figure 1d, and the results show that $T_{d,5\%}$ is 252, 244, and 235 °C and $T_{d,10\%}$ is 272, 276, and 260 °C for PU_{-IPDI}, PU_{-HMDI}, and PU_{-MDI}, possessing good thermal stability, respectively. PU_{-MDI} and PU_{-IPDI} have two obvious two-step thermal degradation processes corresponding to the two peaks of the DTG curve, indicating the first thermal decomposition of the urea groups (PU_{-MDI}: 220−340 °C and PU_{-IPDI}: 220−300 °C) and the second thermal decomposition of the benzene ring or lipid ring (PU_{-MDI}: 340−420 °C and PU_{-IPDI}: 300−420 °C). On comparison, PU_{-HMDI} shows a single-step thermal decomposition with higher residue weight at the temperature range of 220−420 °C, indicating improved thermal

https://doi.org/10.1021/acsami.2c18489
ACS Appl. Mater. Interfaces 2023, 15, 2163−2171

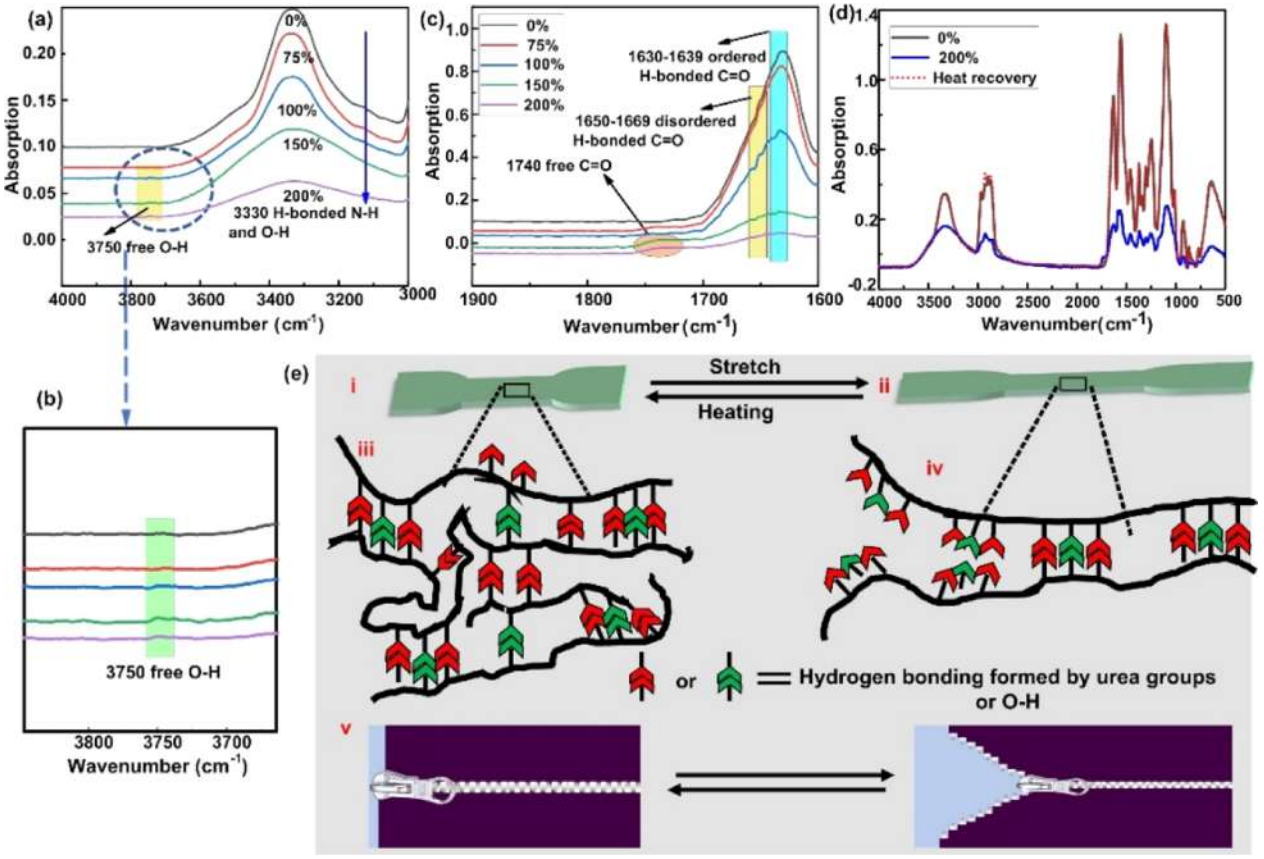

Figure 3. FT-IR spectra of H-bonded N−H (a), free O−H (b), and H-bonded C═O (c) at different strains (0, 75, 100, 150, and 200%). (d) FT-IR spectra of PU_{-HMDI} at different strains (0 and 200%) and heat recovery for characterizing the reversibility of H-bonding. (e) Simulated diagram of molecular network structure changes under external stimuli.

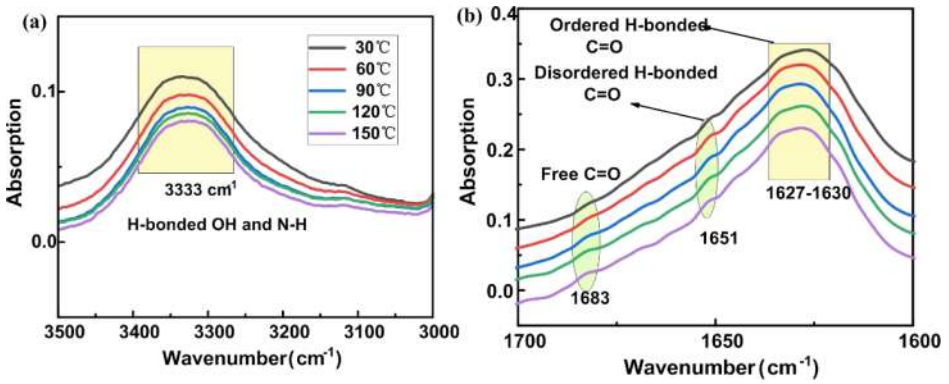

Figure 4. (a) Curve fitting of N−H and C═O stretching regions for PU_{-HMDI} recorded at 30, 60, 90, 120, and 150 °C. (b) Quantitative calculation of H-bonded N−H and C═O and the dissociation ratio of H-bonded N−H and C═O under different temperatures.

stability with a more stable urea bond, which is also reflected by the change of peak (Figure 1d inset) in the derivative weight curves at 300 °C. DSC curves are widely characterized to obtain the phase transitions of polymers and are shown in Figure 1e. PU_{-IPDI}, PU_{-HMDI}, and PU_{-MDI} have only a step peak appearing at 162, 166, and 128 °C, representing the glass-transition temperature. As shown in Figure 1f, the loss modulus demonstrates that T_g is 142, 152, and 110 °C corresponding to PU_{-IPDI}, PU_{-HMDI}, and PU_{-MDI}, respectively, and the storage modulus of PUs is 685, 366, 951 MPa at 30 °C corresponding to PU_{-IPDI}, PU_{-HMDI}, and PU_{-MDI}, respectively. The stress−strain curve can reflect the mechanical strength and toughness of the polymers. The stress−strain curves of the three PUs are shown in Figure 1g. Among them, PU_{-HMDI} has a tensile strength of 51 MPa and an elongation at break of 372%, possessing the highest mechanical strength. Similarly, the tensile strength of PU_{-IPDI} and PU_{-MDI} is 35 and 36 MPa corresponding to the elongation at break of 454 and 255%, respectively, and all are listed in Table 1. This is because the IPDI and MDI with a higher rigidity and shorter chain length leads to decreased extensibility. Further, the molecular network of PU_{-HMDI} has stronger H-bonding interactions, which can dissipate more energy. The three PUs, prepared by engineering a soft and hard phase structure with a multistage H-bonding cross-linked network, possess a splendid trade-off between mechanical robustness and toughness. A sacrificial H-bonding cross-linked network is also able to

https://doi.org/10.1021/acsami.2c18489
ACS Appl. Mater. Interfaces 2023, 15, 2163−2171

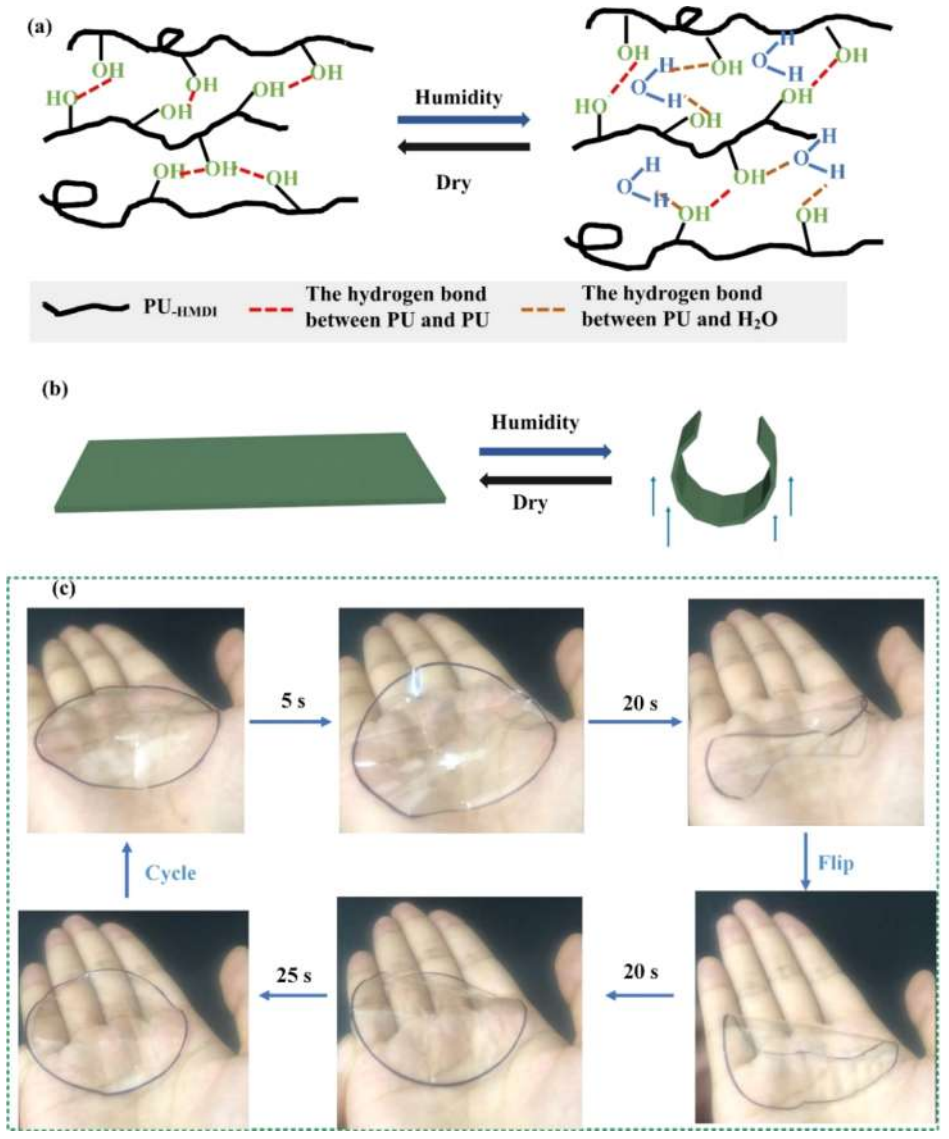

Figure 5. (a) Molecular interactions, particularly hydrogen bonds among PU_{-HMDI}, PU_{-HMDI}, and water molecules under dry−humidity conversion. (b) Schematic of humidity-responsive reversible behavior under dry−humidity conversion. (c) Motion process of the PU_{-HMDI} film on a moist palm.

efficaciously dissipate large amounts of percussive energy by reversible bond rupture, providing effective ability to reversibly recover after large strain.[30,31]

2.2. Dynamic Reversible Network. PU_{-HMDI} is chosen as the object due to its high mechanical performance. Small-angle X-ray scattering (SAXS) is employed to analyze quantificationally the phase-separated structure of soft and hard segments and strain-induced change of network for PU_{-HMDI}. To more intuitively observe the microstructure variation during the stretching process, the 2D SAXS images of PU_{-HMDI} at 0% and 200% strains are shown in Figure 2a,b. The beam spot shape of the film at 0% strain is circular with high homogeneity, which indicates that the network structure is unordered and winding, corresponding to the random network structure shown in Figure 2d. The beam spot shape of the film at 200% strain is elliptic in stretching direction, corresponding to the intuitive arrangement orientation of the network structure along the stretching direction shown in Figure 2e, and the symbol of the network corresponding to the molecular structure is shown in Figure 2f.

In Figure 2c, a strong and narrow scattering peak (q^*) at ~0.505 nm^{-1} is found for PU_{-HMDI}-0%, indicating the existence of phase-separated domains.[32] To further investigate the changes of a strain-induced molecular microstructure, the SAXS patterns of the sample with a strain of 200% are displayed at ~0.449 nm^{-1}, showing lower intensity. The periodicity (D) of the phase-separated domains is calculated by Bragg's law ($D = 2\pi/q^*$).[3,24] The value of D is 12 and 14 nm for $PU_{-HMDI-0\%}$ and $PU_{-HMDI-200\%}$, respectively. The D value for $PU_{-HMDI-200\%}$ is bigger than that for $PU_{-HMDI-0\%}$ due to the dissociation of H-bonding and expansion of entangled molecular chains along with the increase in strain. However, the intensity of the scattering peak is weaker because the dissociation of H-bonding during stretching altered the microstructure, leading to attenuating microphase separation.[15]

2.3. Force-Responsive H-bonding. The Fourier transform infrared (FT-IR) spectrum is an effective and direct way to analyze H-bonding. The effect of thickness on the test results is excluded by normalization, and the normalized results for different thicknesses are shown in Figure S3. To demonstrate the effect of external forces on the molecular structure, PU_{-HMDI} with different strains is characterized by FT-IR spectra. The peak at 3333 cm^{-1} is assigned to H-bonded N−H and O−H, and it is

https://doi.org/10.1021/acsami.2c18489
ACS Appl. Mater. Interfaces 2023, 15, 2163−2171

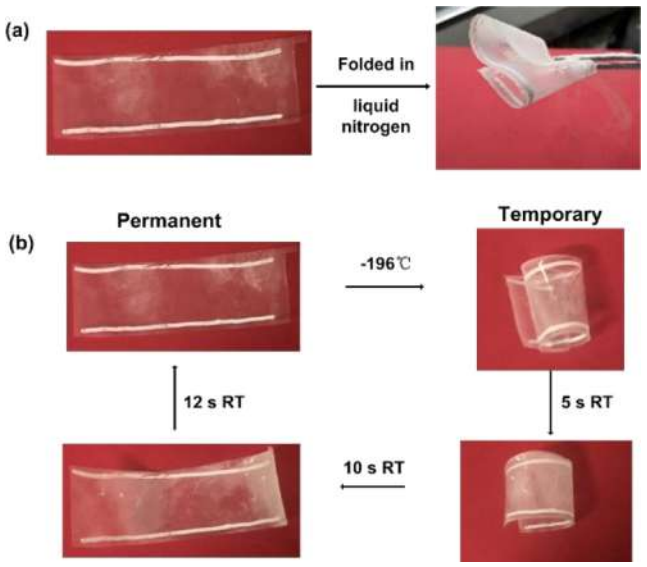

Figure 6. (a) Ductility of PU_{-HMDI} in liquid nitrogen (−196 °C). (b) Shape memory effect of PU_{-HMDI} at room temperature.

clearly shown in Figure 3a that the intensity of the absorption peak decreases gradually with the increase of strain owing to hydrogen bond breaking. Similarly, in Figure 3c, it can be clearly seen that the peak at 1630−1639 cm^{-1} is assigned to ordered H-bonded C═O; when the strain is 0 and 75%, only a strong and narrow absorption peak of C═O is observed at 1633 cm^{-1}. Subsequently, when the strain is increased to 100%, the intensity of the absorption peak decreased obviously at 1633 cm^{-1}, and a new peak appearing at 1652 cm^{-1} is assigned to the disordered H-bonded C═O; further, when the strain is increased to 150 and 200%, the peak becomes weak and wide, indicating more weak H-bonding between molecules. Besides, Figure 3b shows that new peaks appear at 1740 cm^{-1} corresponding to free C═O, and Figure 3d shows that new peaks appear at 3750 cm^{-1} corresponding to free O−H. Therefore, we confirm that the stretching force can pull open intermolecular H-bonding. To prove the reversibility of H-bonding, the FT-IR spectra of the 200% film after the recovery of original shape are compared with those of 0 and 200% strains in Figure 3d, and the FT-IR curve of heat recovery is almost identical to that of 0% strain, indicating that H-bonding possesses high reversibility.

To more intuitively understand the changes in molecular structure under external stimuli, the simulated diagram of molecular network structure changes based on Figures 2 and 3a−d is shown in Figure 3e. Interspersed and tangled chains of molecules become orientated in the direction of the stretching force, corresponding to Figure 3e(iii,iv) equating Figure 2d,e, and the process can be recovered by heating or humidity. The whole process is like a clothing zipper possessing controllable opening and closing shown in Figure 3e(v). H-bonding can be opened by the applied force like an opened zipper and recombined by heating like a closed zipper, which provides a dynamic reversible network structure to improve the mechanical property of PU_{-HMDI}.

2.4. Thermal-Responsive H-Bonding. As an effective method of characterization, variable-temperature Fourier transform infrared (VT-FT-IR) spectra are used to analyze the effect of temperature on H-bonding. As shown in Figure 4a, the peaks of H-bonded N−H and ordered H-bonded OH at 3333 cm^{-1} weaken with increasing temperature because of the thermal-induced dissociation of H-bonding corresponding to a decrease in the absorption value from 0.11 to 0.08. Further, the peak of disordered H-bonded C═O at 1651 cm^{-1} increased slightly with increasing temperature, and the new peaks of free C═O appear and strengthen at 1683 cm^{-1} when the temperature is above 120 °C because part of ordered H-bonded C═O is dissociated into disordered and free states with increasing temperature.[32] To quantitatively analyze the change of intermolecular H-bonding, the curves in Figure 4a were integrated to obtain the curves in Figure 4b. The shifting values of H-bonded N−H (or O−H) and H-bonded C═O against temperature are presented to illustrate the weakened tendency of hydrogen bonding. In addition, the dissociated ratios of H-bonding are calculated, and the dissociated ratios of H-bonded N−H (or O−H) reach 33%, but C═O only reach 5.5% at 150 °C, indicating that the hydrogen bonding formed by urea groups possesses higher thermal stability, and dissociated ratios of the H-bonding formed by O−H hold a much larger percentage at 60−150 °C (Figure S4a, Supporting Information). Further, the change of relaxation modulus indicates that the dynamic network exchanges rapidly at 150 °C (Figure S4b, Supporting Information).

2.5. Humidity-Responsive Actuator. Meaningfully, the novel pure polymer with humidity-responsive and high mechanical properties is different from previous reports that were composite materials such as cellulose or MXene.[3,22,24] It is sensitive to water molecules due to the large number of O−H groups in the molecular structure of PU_{-HMDI}. As shown in Figure 5a, H-bonding of molecular interactions is present among PU_{-HMDI}, PU_{-HMDI}, and water molecules under dry−humidity conversion. In Figure 5b, because the bottom of the PU_{-HMDI} film first absorbs water and expands, leading to a change in the macro shape, the humidity gradient triggers deformation, leading to a bend toward the direction of low humidity to curl away from the humidity surface. When the humidity is off, the film can recover its original shape with volatilization of absorbed water, which is infinitely reversible. To show the PU_{-HMDI} film with good response sensitivity to human humidity, we put the PU_{-HMDI} film on our palm with 65% humidity, as shown in Figure 5c. Clearly, the flat film can quickly curl to 20° in less than 5 s; when the time increases to 20 s, it bends to 160°; then, the film is rolled over under the action of manpower and reversibly recover into 0° (Movie S1, Supporting Information). Adequately, the film will not change on the palm of the gloved hand (Figure S5, Supporting Information), which illustrates that deformation of the film depends on humidity rather than temperature. The response behavior of the PU_{-HMDI} film is created by anisotropic characteristics that the different humidity-absorbing and humidity-releasing capacities of the two sides leads to different expansion rates of the network structure, prompting shape change.[23,33]

2.6. Shape Memory Behavior. *2.6.1. Foldability at −196 °C and Shape Memory Effect in Room Temperature.* High transition temperature has become the focus of SMP research to apply in high temperature, intense radiation, aerospace, and other complex fields.[34−36] However, few research studies have reported on ultralow-temperature plastic/elastic SMPs that are also urgently needed in extremely cold environments such as Antarctica, Moon, and Mars.[37] At −196 °C, PU_{-HMDI} preserves an optically transparent and mechanically ductility in Figure 6a. To qualitatively characterize the low-temperature resistance of PU_{-HMDI}, PU_{-HMDI} is submerged in liquid nitrogen and folded under the action of a large external force. The rectangular film is

https://doi.org/10.1021/acsami.2c18489
ACS Appl. Mater. Interfaces 2023, 15, 2163−2171

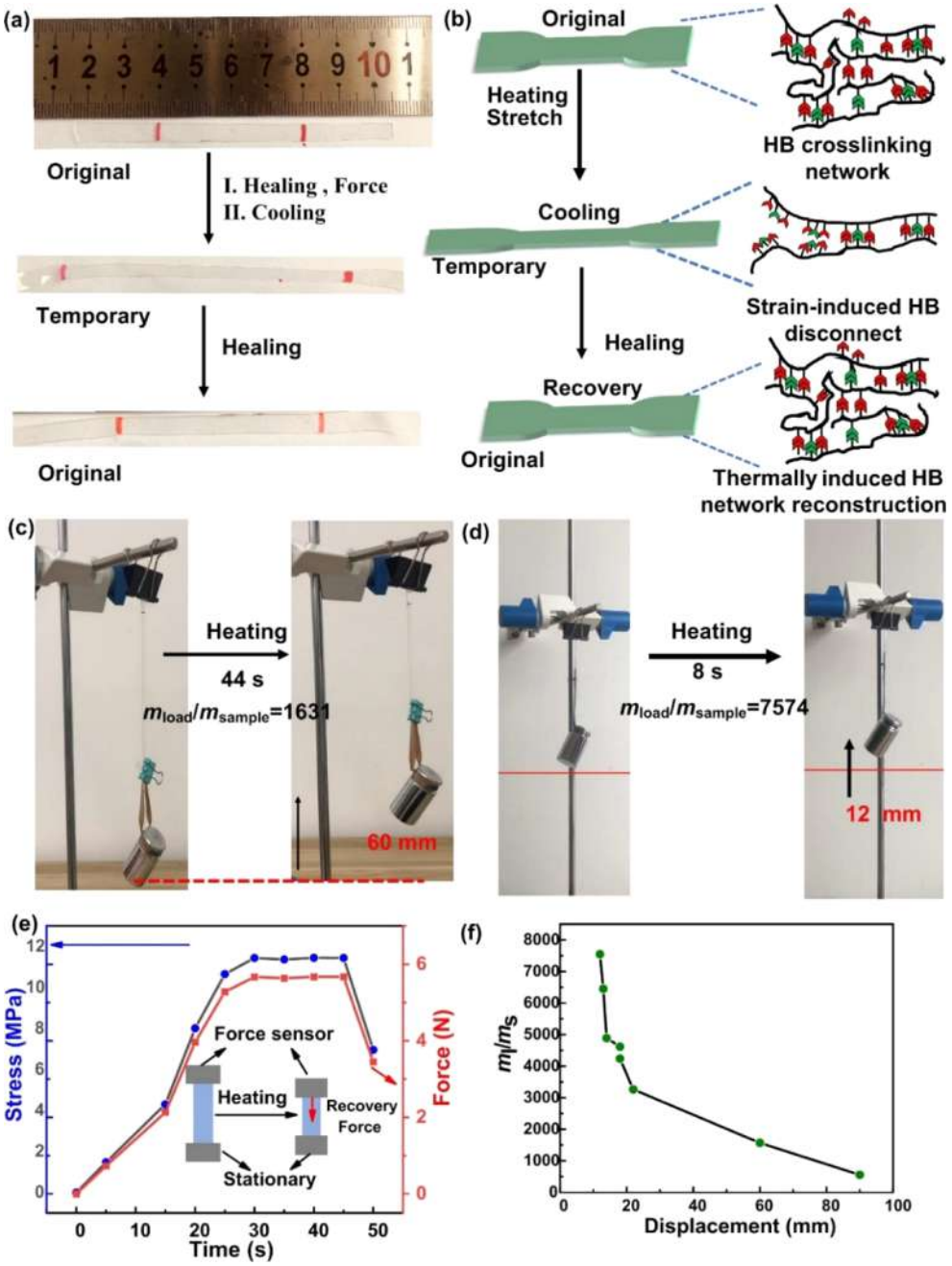

Figure 7. (a) Shape memory process of PU_{-HMDI}. (b) Corresponding changes of the structure of PU_{-HMDI}. (c) Photos of a PU_{-HMDI} strip lifting 100 g weight up 60 mm. (d) Photos of a PU_{-HMDI} strip lifting 200 g weight up 12 mm by employing a heating gun. (e) Curve of recovery stress and force with time by employing a heating gun. (d) Different m_{load}/m_{sample} corresponding to displacement in the shape recovery process.

placed in liquid nitrogen, and it can be folded to arbitrary shape without breaking like "S" shape, indicating that PU_{-HMDI} still possesses excellent flexibility at −196 °C (Movie S2, Supporting Information). Besides, "360° the towel roll" shape fixed in liquid nitrogen is able to unfold into a "0° plane" shape at room temperature in only 12 s (Movie S3, Supporting Information), which is a very potentially valuable and reusable building material in extremely cold environments.

2.6.2. Actuation Performance. Subsequently, PU_{-HMDI} demonstrates a high energy output in the shape recovery process under thermal stimulus. Figure 7a shows a pre-stretched film with 100% strain as a temporary recovery original shape with 90% shape recovery ratio, corresponding to the dynamic variation of the network structure in Figure 7b. The high energy output of SMPs simultaneously possesses high recovery stress and large recoverable strain. The recovery stress is determined by the stored entropic energy in the network being controlled by the density and strength of network junctions.[9] The multiple H-bonding cross-linked network possessing the adjustable strong and weak segments is able to increase high steric hindrance or intermolecular interactions to increase the density and strength of network junctions and balance the conflict between strength and toughness to ensure large recoverable strain.[38] Therefore, the pre-stretched film possesses more high energy output to lift weight. For example, in Figure 7c, it is shown that the pre-strained PU_{-HMDI} raised a 100 g weight exceeding 1631 times its

https://doi.org/10.1021/acsami.2c18489
ACS Appl. Mater. Interfaces 2023, 15, 2163−2171

own mass by a heat gun, producing a distance of up 60 mm at 44 s (Movie S4, Supporting Information) and 0.98 J/g work output (29.7 times that of human skeletal muscles) according to the calculation equation:

$$w = \frac{m_{load} \times g \times (L_2 - L_3)}{m_{sample}} \quad (1)$$

where m_{load} and m_{sample} represent the mass of the load and the sample, respectively. L_2 represents the fixation length after removing the external force from heating to cooling, and L_3 represents the final length after the shape recovery process. Meanwhile, g represents the acceleration of gravity, and its value is 10 N/kg. In Figure 7d, the pre-strained PU_{-HMDI} lifts a 200 g weight exceeding 7547 times its own mass up 12 mm by a heat gun for 5 s, possessing 0.91 J/g work output. In Figure 7e, the value of recovery stress with time is shown, and the biggest value reaches 12 MPa. The upward displacement of the weight is associated with m_{load}/m_{sample}. When m_{load}/m_{sample} is 556, the upward displacement is 90 mm, as shown in Figure 7f. In a word, PU_{-HMDI} not only has the shape memory effect at low temperature but also has high energy density during shape recovery at high temperature, which produces a higher energy output employed as an artificial muscle actuator.

3. CONCLUSIONS

In summary, we develop a tough and robust polyurea hard plastic, equipping with a unique molecular network structure of reversible H-bonding cross-linking and mechanical force response. Besides, the high transparency polyurea shows humidity-controlled deformation ability and heat-induced shape memory behavior, which produce a high energy output as an artificial muscle actuator. Owing to reversible H-bonding cross-linking, the molecular structure of PU_{-HMDI} can be opened under mechanical force and re-bonded under heating like a zipper, which can adjust the strength and toughness of PU_{-HMDI}. Furthermore, because PU_{-HMDI} possesses a remarkable humidity-responsive behavior, it can automatically fold up 120° only 30 s in the palm. Meanwhile, through the shape recovery process, the PU_{-HMDI} film can lift 100 g weight (own weight 1631 times) up 60 mm and lift 200 g weight (own weight 7547 times) up 12 mm. Finally, PU_{-HMDI} still keeps excellent malleability in −196 °C and shows shape recovery behavior at room temperature. These demonstrations clearly indicate that PU_{-HMDI} is promising for a large deployable structure in extreme environments, artificial muscle actuators, wearable humidity sensors, and smart skin.

4. EXPERIMENTAL SECTION

4.1. Materials. Poly(propylene glycol) bis(2-aminopropyl ether) (ED, Mn = 2000 g mol^{-1}), isophorone diisocyanate (IPDI, 99%), methylene-bis(4-cyclohexylisocyanate) (HMDI, 90%), and *N*,*N*-dimethylacetamide (DMAc, 99.8%) were purchased from Macklin (China). 1,3-Diamino-2-propanol (DMPP, 97%) and 4,4′-MDI (MDI, 98%) were purchased from Aladdin (China).

4.2. Preparation of PU. DMAc was drastically dried by the 4A molecular sieve for about 48 h, and ED2000 was dehydrated by keeping for 1 h at 120 °C under vacuum. The typical synthetic routes for PU_{-IPDI}, PU_{-HMDI}, and PU_{-MDI} were described in detail as follows. For example, the preparation process of PU_{-IPDI} was introduced in detail. IPDI (2.22 g) and ED2000 (2.4752 g) were dissolved in 2 and 3 mL of DMAc, respectively, followed by dropping the ED2000 solution into the IPDI solution at room temperature and stirring for 0.5 h; subsequently, a solution of 0.7797 g of DMPP dissolved 10 mL of DMAc was dropped in the prepolymer solution, keeping the reaction for 12 h at room temperature. The resulting viscous reaction solution was poured into deionized water, precipitating a white product that was then washed three times with ethanol and dried for later use. It should be noted that HMDI and MDI were more highly reactive. Therefore, DMPP was dropped in the prepolymer solution, keeping the reaction in an ice bath.

4.3. Characterization. FT-IR spectra were employed to characterize the molecular structure and intermolecular interactions by a PerkinElmer SPECTRUM ONE with the scanning range from 4000 to 400 cm^{-1}. VT-FT-IR spectra were recorded using a Thermo Fisher Nicolet IS50 Fourier transform infrared spectrometer, the test method was ATR, and the test temperatures were 30, 60, 90, 120, and 150 °C. Dynamic mechanical analysis Q800 (DMA) was carried out to test the storage modulus and glass-transition temperature. Different scanning calorimetry (DSC) thermal analysis was performed on a DSC 1 STAR System from 25 to 180 °C at a rate of 10 °C/min. TGA was performed from 25 to 800 °C at a rate of 10 °C/min in N_2.

4.4. Characterization of Hydrogen Bonding Reversibility. First, the films with 0, 75, 100, 150, and 200% strain were tested by FT-IR spectra. Then, they were heated on a hot plate to recover the original shape, which were tested again by FT-IR spectra. By analyzing the change of characteristic peak strength and position, the force response and reversible performance of the hydrogen bond were proved.

4.5. Tensile Testing. Universal testing machine Zwick Z010 (Zwick Roell) was used for the tensile tests. Rectangular samples with an approximate dimension of 15 mm × 5 mm × 0.2 mm were cut from the substrate, and the strain rate was 30 mm/min at room temperature.

4.6. SAXS Testing. An Austria Anton Paar SaxsPoint 2.0 SAXS system was employed for SAXS, equipped with a Cu Kα radiation source and a wavelength of 0.154 nm, and the test scattering range was 0.07−3 nm^{-1} with an accuracy of 0.005 nm^{-1}.

■ ASSOCIATED CONTENT

Supporting Information

The Supporting Information is available free of charge at https://pubs.acs.org/doi/10.1021/acsami.2c18489.

PU_{-HMDI} film with response sensitivity on the palm (MP4)

PU_{-HMDI} film with excellent flexibility in liquid nitrogen (MP4)

PU_{-HMDI} film of the shape memory process at room temperature (MP4)

PU_{-HMDI} film lifting the load its mass 1631 times moving up 60 mm by a heat gun (MP4)

FTIR spectra of N−H; FT-IR spectra of C═O; FTIR curves of two thicknesses after normalization; quantitative calculation of hydrogen bonding; and film on the palm of the gloved hand (PDF)

■ AUTHOR INFORMATION

Corresponding Author

Jinsong Leng − *Center for Composite Materials and Structures, Harbin Institute of Technology, 150080 Harbin, P. R. China;* orcid.org/0000-0001-5098-9871; Email: lengjs@hit.edu.cn

Authors

Wen Liu − *Center for Composite Materials and Structures, Harbin Institute of Technology, 150080 Harbin, P. R. China*

Yang He − *Center for Composite Materials and Structures, Harbin Institute of Technology, 150080 Harbin, P. R. China*

Complete contact information is available at: https://pubs.acs.org/10.1021/acsami.2c18489

Funding

This work was funded by the National Key R&D Program of China (2022YFB3805700).

Notes

The authors declare no competing financial interest.

REFERENCES

(1) Pan, X.; Zhang, Y.; Lu, Y.; Yang, F.; Yue, H. A Reusable SMA Actuated Non-explosive Lock-release Mechanism for Space Application. *Int Int. J. Smart Nano Mater.* **2020**, *11*, 65.

(2) Lin, C.; Liu, L.; Liu, Y. J.; Leng, J. S. 4D Printing of Bioinspired Absorbable Left Atrial Appendage Occluders: A Proof-of-Concept Study. *ACS Appl. Mater. Interfaces* **2021**, *13*, 12668−12678.

(3) Zhang, Z. H.; Chen, Z. Y.; Wang, Y.; Zhao, Y. J.; Shang, L. R. Cholesteric Cellulose Liquid Crystals with Multifunctional Structural Colors. *Adv. Funct. Mater.* **2021**, *32*, 2107242.

(4) Lei, Y.; Wang, Y.; Yuan, A. Q.; Zhao, S. W.; Chen, Y.; Xiao, Y.; Jiang, L.; Lei, J. X. Solving the Difficult Recyclability of Conventional Thermosetting Polyurea Elastomers Based on Commercial Raw Materials in a Facile Way. *J. Mater. Chem. A* **2022**, *10*, 6713−6723.

(5) Chen, C.; Liu, Y.; He, X.; Li, H.; Chen, H.; Wei, Y.; Zhao, Y.; Ma, Y.; Chen, Z.; Zheng, X.; Liu, H. Multiresponse Shape-Memory Nanocomposite with a Reversible Cycle for Powerful Artificial Muscles. *Chem. Mater.* **2021**, *33*, 987−997.

(6) Li, A.; Fan, J.; Li, G. Recyclable Thermoset Shape Memory Polymers with High Stress and Energy Output via Facile UV-curing. *J. Mater. Chem. A* **2018**, *6*, 11479−11487.

(7) McCracken, J. M.; Donovan, B. R.; White, T. J. Materials as Machines. *Adv. Mater.* **2020**, *32*, No. e1906564.

(8) Xia, Y. L.; He, Y.; Zhang, F. H.; Liu, Y. J.; Leng, J. S. A Review of Shape Memory Polymers and Composites: Mechanisms, Materials, and Applications. *Adv. Mater.* **2021**, *33*, No. e2000713.

(9) Cooper, C. B.; Nikzad, S.; Yan, H.; Ochiai, Y.; Lai, J. C.; Yu, Z.; Chen, G.; Kang, J.; Bao, Z. High Energy Density Shape Memory Polymers Using Strain-Induced Supramolecular Nanostructures. *ACS Cent. Sci.* **2021**, *7*, 1657−1667.

(10) Lang, C.; Lloyd, E. C.; Matuszewski, K. E.; Xu, Y.; Ganesan, V.; Huang, R.; Kumar, M.; Hickey, R. J. Nanostructured Block Copolymer Muscles. *Nat. Nanotechnol.* **2022**, *17*, 752−758.

(11) Chung, W. J.; Oh, J. W. K.; Kwak, B. Y.; Lee, J.; Meyer, E.; Wang, A.; Hexemer, S. W.; Lee, S.-W. Biomimetic Self-templating Supramolecular Structures. *Nature* **2011**, *478*, 364−368.

(12) Zan, G.; Wu, Q. Biomimetic and Bioinspired Synthesis of Nanomaterials/Nanostructures. *Adv. Mater.* **2016**, *28*, 2099−2147.

(13) Li, Z.; Zhu, Y. L.; Niu, W.; Yang, X.; Jiang, Z.; Lu, Z. Y.; Liu, X.; Sun, J. Healable and Recyclable Elastomers with Record-High Mechanical Robustness, Unprecedented Crack Tolerance, and Superhigh Elastic Restorability. *Adv. Mater.* **2021**, *33*, No. e2101498.

(14) Du, X.; Cui, H.; Zhao, Q.; Wang, J.; Chen, Y.; Wang, Y. Inside-Out 3D Reversible Ion-Triggered Shape-Morphing Hydrogels. *Research* **2019**, *2019*, 1−12.

(15) Wang, X. Y.; Xu, J.; Zhang, X. R.; Yang, Z. H.; Zhang, Y. M.; Wang, T. M.; Wang, Q. H. Molecularly Engineered Unparalleled Strength and Super Toughness Poly(urea-urethane) with Shape Memory and Clusterization-triggered Emission. *Adv. Mater.* **2022**, *34*, No. e2205763.

(16) Wei, J.; Li, R.; Li, L.; Wang, W.; Chen, T. Touch-Responsive Hydrogel for Biomimetic Flytrap-Like Soft Actuator. *Nanomicro Lett* **2022**, *14*, 1−13.

(17) Arazoe, H.; Miyajima, D.; Akaike, K.; Araoka, F.; Sato, E.; Hikima, T.; Kawamoto, M.; Aida, T. An Autonomous Actuator Driven by Fluctuations in Ambient Humidity. *Nat. Mater.* **2016**, *15*, 1084−1089.

(18) Li, Q. Y.; Sun, RJ.; Le Duigou, A.; Guo, J. L.; Rossiter, J.; Liu, L. W.; Leng, J. S.; Scarpa, F. Programmable and Reconfigurable Hygro-Thermo Morphing Materials with Multifunctional Shape Transformation. *Appl. Mater. Today* **2022**, *27*, 101414.

(19) Wang, H.; Liu, Z. L.; Lao, J.; Zhang, S.; Abzalimov, R.; Wang, T.; Chen, X. High Energy and Power Density Peptidoglycan Muscles through Super-Viscous Nanoconfined Water. *Adv. Sci.* **2022**, *9*, No. e2104697.

(20) Chen, L. R.; Chang, X. H.; Wang, H. C.; Chen, J. W.; Zhu, Y. Stretchable and Transparent Multimodal Electronic-skin Sensors in Detecting Strain, Temperature, and Humidity. *Nano Energy* **2022**, *96*, 107077.

(21) Islam, M. R. X.; Li, K.; Smyth, M. J.; Serpe, M. J. Polymer-Based Muscle Expansion and Contraction. *Angew. Chem., Int. Ed.* **2013**, *52*, 10330−10333.

(22) Cai, G. F.; Ciou, H. J.; Liu, Y. Z.; Jiang, Y.; Lee, P. S. Leaf-Inspired Multiresponsive MXene-Based Actuator for Programmable Smart Devices. *Sci. Adv.* **2019**, *5*, No. eaaw7956.

(23) Wang, J.; Liu, Y.; Cheng, Z.; Xie, Z.; Yin, L.; Wang, W.; Song, Y.; Zhang, H.; Wang, Y.; Fan, Z. Highly Conductive MXene Film Actuator Based on Moisture Gradients. *Angew. Chem., Int. Ed.* **2020**, *59*, 14029−14033.

(24) Han, D. D.; Liu, Y. Q.; Ma, J. N.; Mao, J. W.; Chen, Z. D.; Zhang, Y. L.; Sun, H. B. Biomimetic Graphene Actuators Enabled by Multiresponse Graphene Oxide Paper with Pretailored Reduction Gradient. *Adv. Mater. Technol.* **2018**, *3*, 1800258.

(25) Zhang, L.; Liang, H.; Jacob, J.; Naumov, P. Photogated Humidity-Driven Motility. *Nat. Commun.* **2015**, *6*, 7429.

(26) Zhang, K.; Geissler, A.; Standhardt, M.; Mehlhase, S.; Gallei, M.; Chen, L.; Marie Thiele, C. Moisture-Responsive Films of Cellulose Stearoyl Esters Showing Reversible Shape Transitions. *Sci. Rep.* **2015**, *5*, 11011.

(27) Xue, J.; Ge, Y.; Liu, Z.; Liu, Z.; Jiang, J.; Li, G. Photoprogrammable Moisture-Responsive Actuation of a Shape Memory Polymer Film. *ACS Appl. Mater. Interfaces* **2022**, *14*, 10836−10843.

(28) Liu, W.; He, Y.; Leng, J. Shape Memory Supramolecular Polyurea with Adjustable Toughness and Ultrahigh Energy Density. *ACS Appl. Polym. Mater.* **2022**, *4*, 6092−6102.

(29) Song, Y.; Liu, Y.; Qi, T.; Li, G. L. Towards Dynamic but Supertough Healable Polymers through Biomimetic Hierarchical Hydrogen-Bonding Interactions. *Angew. Chem., Int. Ed.* **2018**, *57*, 13838−13842.

(30) Neal, J. A.; Mozhdehi, D.; Guan, Z. Enhancing Mechanical Performance of a Covalent Self-Healing Material by Sacrificial Noncovalent Bonds. *J. Am. Chem. Soc.* **2015**, *137*, 4846−4850.

(31) Song, P.; Wang, H. High-Performance Polymeric Materials through Hydrogen-Bond Cross-Linking. *Adv. Mater.* **2020**, *32*, No. e1901244.

(32) Chen, X.; Zawaski, C. E.; Spiering, G. A.; Liu, B.; Orsino, C. M.; Moore, R. B.; Williams, C. B.; Long, T. E. Quadruple Hydrogen Bonding Supramolecular Elastomers for Melt Extrusion Additive Manufacturing. *ACS Appl. Mater. Interfaces* **2020**, *12*, 32006−32016.

(33) Yang, L. Y.; Cui, J. Z.; Zhang, X.; Xu, X. R.; Chen, S.; Sun, D. A Moisture-Driven Actuator Based on Polydopamine-Modified MXene/Bacterial Cellulose Nanofiber Composite Film. *Adv. Funct. Mater.* **2021**, *31*, 2101378.

(34) Xiao, X.; Kong, D.; Qiu, X.; Zhang, W.; Liu, Y.; Zhang, S.; Zhang, F.; Hu, Y.; Leng, J. Shape Memory Polymers with High and Low Temperature Resistant Properties. *Sci. Rep.* **2015**, *5*, 14137.

(35) Feng, X.; Li, G. High-Temperature Shape Memory Photopolymer with Intrinsic Flame Retardancy and Record-high Recovery Stress. *Appl. Mater. Today.* **2021**, *23*, 101056.

(36) Ma, Q.; Liao, S.; Ma, Y.; Chu, Y.; Wang, Y. An Ultra-Low-Temperature Elastomer with Excellent Mechanical Performance and Solvent Resistance. *Adv. Mater.* **2021**, *33*, No. e2102096.

(37) Hu, J. Y.; Jiang, N.; Du, J. K. Thermally Controlled Large Deformation in Temperature-Sensitive Hydrogels Bilayers. *Int. J. Smart Nano Mater.* **2021**, *12*, 450−471.

(38) Qi, X. M.; Dong, Y. B.; Islam, M. D.; Zhu, Y. F.; Fu, Y. Q.; Fu, S. Y. Excellent Triple-Shape Memory Effect and Superior Recovery Stress of Ethylene-vinyl Acetate Copolymer Fiber. *Compos. Sci. Technol.* **2021**, *203*, 108609.

https://doi.org/10.1021/acsami.2c18489
ACS Appl. Mater. Interfaces 2023, 15, 2163−2171